Chemical Science

ROYAL SOCIETY OF CHEMISTRY

EDGE ARTICLE

View Article Online
View Journal | View Issue

Cite this: *Chem. Sci.*, 2024, **15**, 15804

All publication charges for this article have been paid for by the Royal Society of Chemistry

Received 9th June 2024
Accepted 27th August 2024

DOI: 10.1039/d4sc03778b

rsc.li/chemical-science

Introduction of the $-B(OH)_2$ group into a graphene motif for p_z orbital removal and ferromagnetic modulation†

Di Zhang,‡[a] Bo Gao,‡[a] Yuqi Ouyang,[a] Song Xu, *[b] Qingyong Tian,[b] Wenzhuo Wu[b] and Qun Xu *[ab]

Room-temperature ferromagnetism in graphene has attracted considerable attention due to its potential application as spintronics. Theoretically, magnetic moment of graphene can be generated by removing a single p_z orbital from the π system, which introduces an unpaired electron into the graphene motif for magnetic coupling. In this work, p_z orbital of graphene is experimentally removed by cleaving the π bond of graphene using H_3BO_3 with the assistance of supercritical CO_2 (SC CO_2), which simultaneously introduces $-B(OH)_2$ groups and unpaired electrons. As a result, ferromagnetic coupling between unpaired electrons substantially enhances the magnetic properties of the 2D graphene motif, leading to room-temperature ferromagnetism. Overall, unpaired electrons were introduced into a 2D graphene motif through π bond cleavage, which provides a novel approach for magnetic manipulation of 2D materials with conjugated structures.

Introduction

Magnetism with a two-dimensional (2D) limit has always been a fascinating topic in condensed matter physics because it offers great potential for next-generation electronic devices and spectroscopic characterizations.[1–3] Due to their extraordinary carrier mobility, long spin diffusion length, weak intrinsic spin–orbit coupling, and limited hyperfine interactions,[4–7] 2D materials including graphene exhibit a series of novel magnetic properties including room-temperature ferromagnetism, disordered magnetism, and magnetoresistance.[8,9] However, conventional graphene lacks an unpaired spin and is therefore nonmagnetic. Prior to this work, various strategies including defect engineering,[10] sp^3 functionalization,[11] chemical doping,[12–14] and surface adsorption[15] have been attempted to introduce unpaired spin into the graphene motif. Subsequently, magnetic coupling between unpaired spins through the fully conjugated graphene motif leads to novel magnetic properties.[16,17]

The introduction of unpaired spin through conventional approaches is generally concomitant with the formation of excessive defects and structural damage, which disrupt the intactness of the conjugated structure and suppress the exchange interactions between the unpaired spins.[18,19] Brihuega *et al.* reported a sophisticated approach to introduce unpaired spin into a graphene motif for ferromagnetic coupling through the deposition of single H atom, which effectively prevents undesired structural damage.[15] Specifically, the p_z orbitals from the π system of graphene are effectively removed by H deposition, leading to the formation of unpaired spins and net magnetic moment based on Lieb's theorem.[20] However, removing p_z orbitals and introducing unpaired spin in a facile and controlled manner remains challenging.

From a fundamental organic chemistry perspective, one of the most straightforward approaches for removing a p_z orbital from a π system is alkene addition, which cleaves C=C bonds and converts the p_z and sp^2 orbitals of C atoms to sp^3 orbitals. As a set of well-established reagents for alkene addition, borane compounds are capable of breaking the C=C bond, leading to conversion from p_z orbital to sp^3 orbital.[21] Apart from alkene addition, the introduction of B-containing functional groups into conjugated 2D materials for magnetic manipulation is relatively well-documented. For example, the bridging –B(OH) group can be introduced into 2D graphite carbon nitride (g-C_3N_4) through supercritical CO_2 (SC CO_2) treatment using H_3BO_3 as the B source, which facilitates the long-range magnetic sequence for room-temperature ferromagnetism.[22]

As a typical conjugated system, 2D graphene is noteworthy because it contains abundant C=C bonds, which serves as an ideal platform for addition reaction. Therefore, introducing B-containing groups into the graphene motif through chemical addition is proposed to be an effective approach for p_z orbital

[a]College of Materials Science and Engineering, Zhengzhou University, Zhengzhou 450052, P.R. China. E-mail: qunxu@zzu.edu.cn

[b]Henan Institute of Advanced Technology, Zhengzhou University, Zhengzhou 450052, P.R. China. E-mail: song24xu11@zzu.edu.cn

† Electronic supplementary information (ESI) available. See DOI: https://doi.org/10.1039/d4sc03778b

‡ These authors are contributed equally to this work.

removal and unpaired spin introduction. However, 2D graphene layers are prone to be stacked as multilayered graphite due to π stacking, which hinders the exposure of C=C bonds for subsequent reactions.

In this work, a facile supercritical CO_2 (SC CO_2)/H_3BO_3/H_2O_2 treatment is utilized to exfoliate bulk graphite into few-layered graphene nanosheets. Subsequently, terminal –$B(OH)_2$ groups were introduced into the graphene motif through π bond cleavage, which removes the p_z orbital and introduces unpaired spin into the system, leading to room-temperature ferromagnetism with saturation magnetization (M_s) up to 0.39 emu g^{-1} at 300 K.

Theoretical calculations attribute the room-temperature ferromagnetism to the ferromagnetic coupling of the unpaired electrons in the as-prepared graphene motif, which is generated from the simultaneous π bond cleavage and –$B(OH)_2$ introduction. In addition to a novel approach to generate ferromagnetic ordering in graphene-derived materials, we anticipate that this work will provide an in-depth understanding of the magnetic origin of 2D materials with conjugated structures.

Results and discussion

Terminal –$B(OH)_2$-containing graphene oxide nanosheets were prepared by a facile supercritical CO_2 (SC CO_2) treatment in the presence of H_3BO_3, where SC CO_2 is expected to exfoliate bulk graphite into graphene nanosheets and boric acid is expected to serve as the B source (Fig. 1a). Considering the presence of the C=C bonds in the graphene motif and the empty p_z orbital in B, the introduction of a terminal –$B(OH)_2$ group was expected to be accomplished by an alkene addition-derived reaction, as shown in Fig. 1b. The product after the SC CO_2 treatment is denoted by B-GO-*X* MPa, where B and *X* refer to the B atom and the pressure of supercritical CO_2, respectively. The introduction of terminal –$B(OH)_2$ was expected to cleave the π bond of graphene, which would effectively remove the p_z orbital from the π-conjugated system, leading to the formation of unpaired electrons for a net magnetic moment (Fig. 1c).

The structure of B-GO-*X* MPa prepared under different pressures was characterized using transmission electron microscopy (TEM) and high-resolution TEM (HRTEM). Prior to the SC CO_2 treatment, well-defined lattice fringes were observed in the ultrasonicated graphite precursor, which was consistent with findings from the literature (Fig. 2a).[23] After SC CO_2 treatment under 12 MPa and 14 MPa, coexistence of crystalline and amorphous graphite was observed for B-GO-*X* MPa ($X = 12$ and 14), based on HRTEM characterization (Fig. 2b and c), where diffracted spots and rings can be observed according to fast Fourier transformation (FFT) analysis. When the pressure reached 16 MPa, well-defined lattice fringes and diffraction

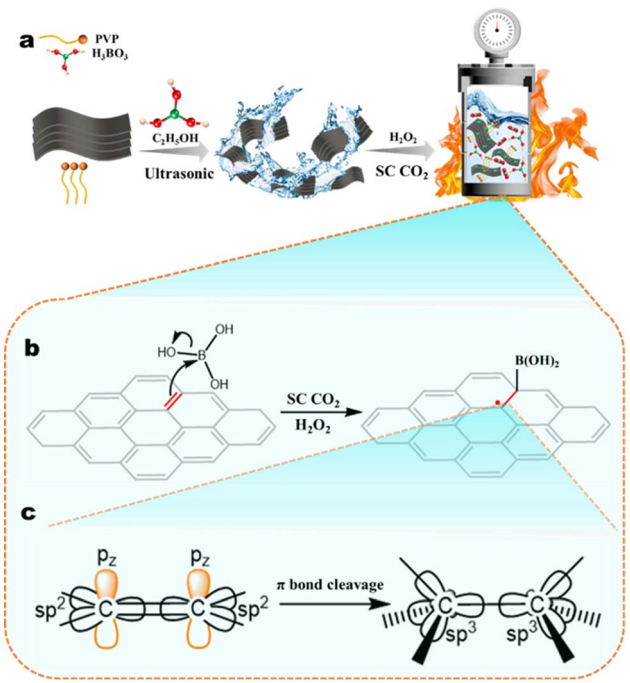

Fig. 1 (a) Schematic illustration of B-GO-*X* MPa preparation through SC CO_2 treatment. (b) Proposed reaction mechanism for –$B(OH)_2$ introduction into the graphene motif. (c) Proposed conversion of p_z and sp^2 to sp^3 orbitals through alkene addition-derived reaction.

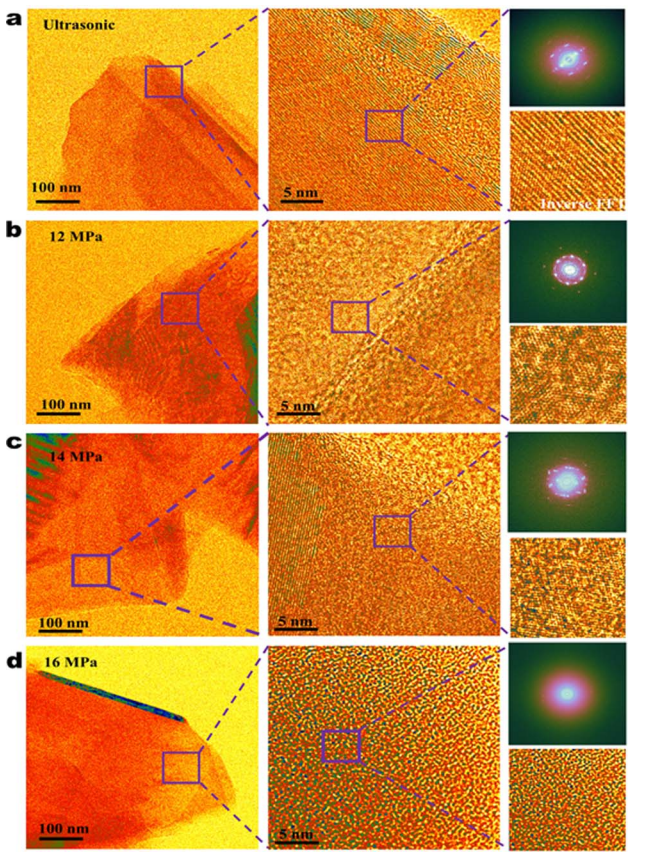

Fig. 2 Characterizations of graphene nanosheets showing TEM images (left), HRTEM images (middle), and selected area diffraction obtained by FFT (right) under different conditions: (a) ultrasonicated graphite, (b) SC CO_2 at 12 MPa, (c) SC CO_2 at 14 MPa, and (d) SC CO_2 at 16 MPa.

spots disappeared for B-GO-16 MPa, suggesting complete amorphization of B-GO-*X* MPa (Fig. 2d).[24]

The thickness and lateral size of B-GO-*X* MPa nanosheets were further characterized by atomic force microscopy (AFM). As shown in Fig. S1,† the thickness and lateral size decreased after SC CO_2 treatment, which is consistent with the introduction of CO_2 into the vdW gap and exfoliation of 2D materials.[22,25,26] Notably, a significant reduction of thickness and lateral size were observed under elevated SC CO_2 pressure, indicating more effective exfoliation and exposure of C=C bonds. As a result, it is expected that additional C=C bonds would be exposed to facilitate the alkene addition-derived reaction shown in Fig. 1b, leading to more effective introduction of $-B(OH)_2$.

The amorphization of B-GO-*X* Pa was further characterized by X-ray diffraction (XRD), where a sharp peak at 26.52° appeared for pristine graphite ultrasonicated with H_3BO_3, which is consistent with the characteristic (002) crystalline plane of graphene (Fig. S2a†).[27,28] When SC CO_2 was applied at different pressures, all diffraction peaks disappeared (Fig. S2b†), which was consistent with the amorphization process characterized by TEM. Nonetheless, the amorphization observed by TEM and XRD indicates introduction of functional groups into the graphene motif, which leads to structural transformation from crystalline to amorphous.[29,30]

Subsequently, the electronic structure of B-GO-*X* Pa was characterized by X-ray photoelectron spectroscopy (XPS). As shown in Fig. 3, only peaks for C 1s and O 1s were observed for graphite sonicated in the presence of H_3BO_3, suggesting that sonication alone cannot introduce B-containing functional groups into the graphene motif. When the graphite precursor is treated with H_3BO_3 under SC CO_2, characteristic peaks of B 1s with binding energies at 193.1 and 190.4 eV were observed for B-GO-*X* MPa, which were attributed to the B atoms connected to O and C atoms (B–O and B–C),[31,32] respectively. Thus, it is plausible to propose that B-hydroxyl functional groups were introduced into graphene during the SC CO_2 treatment, based on XPS characterizations (Fig. S3† and 3a).[33,34]

Consistent with the XPS results for elemental B, a peak corresponding to the B–O moiety at 531.3 eV was observed in the O 1s spectra of B-GO-*X* MPa (Fig. 3b).[22] According to XPS characterizations, B-hydroxyl groups can be introduced into the graphene motif more effectively under higher SC CO_2 pressure, which can be rationalized by the enhancement of graphite exfoliation. As shown in Fig. S1,† the exfoliation of graphite under SC $CO_2/H_3BO_3/H_2O_2$ treatment can be facilitated by increasing SC CO_2 pressure, leading to more effective C=C bond exposure for subsequent reactions. As a result, it is expected that the alkene addition-derived reaction (Fig. 1b) would be facilitated under elevated SC CO_2 pressure, leading to more effective introduction of B-hydroxyl into the graphene motif.

In addition to XPS characterizations of B and O, C 1s spectra of B-GO-*X* MPa were characterized, where the peak of O–C=O (carbonyl) at 288.4 eV appeared under SC CO_2 treatment, concomitant with the growth of the C–OH and C–O (epoxy/phenol hydroxyl) groups at 285.6 and 286.8 eV, respectively (Fig. 3c).[30,35,36] The XPS characterization of elemental O suggests that, in addition to B-hydroxyl groups, other oxygen-containing groups can be simultaneously introduced into graphene *via* SC CO_2/H_3BO_3 treatment.

The introduction of a B-hydroxyl group was further characterized by Raman spectroscopy. Prior to the SC CO_2 treatment, only two characteristic peaks were observed at 1574 and 2695 cm^{-1}, which were attributed to the G and 2D bands of graphene, respectively (Fig. 4a).[37] Notably, characteristic D bands at 1342 cm^{-1} appeared for B-GO-*X* MPa after SC CO_2/H_3BO_3 treatment, while the intensity ratio of the D to G band (I_D/I_G) increased as the pressure of SC CO_2 increased (Fig. S4†).[38] As the G and D bands were attributed to the in-plane vibration

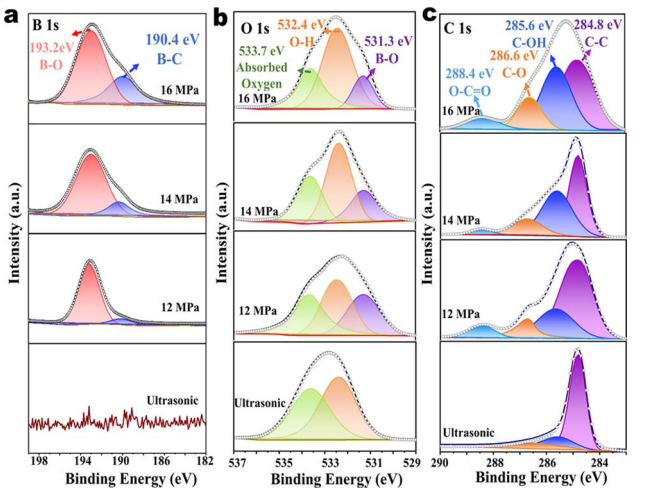

Fig. 3 (a) XPS of the B 1s region of ultrasonicated graphite and B-GO-*X* MPa. (b) XPS of the O 1s region of ultrasonicated graphite and B-GO-*X* MPa. (c) XPS of the C 1s region of ultrasonicated graphite and B-GO-*X* MPa.

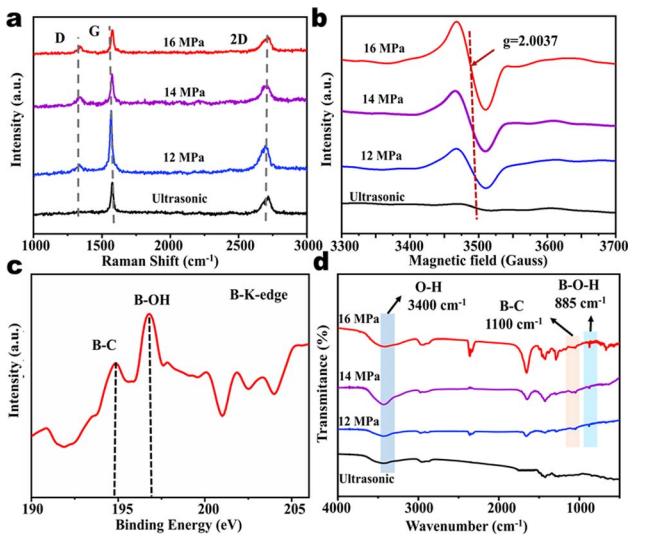

Fig. 4 (a) Raman spectra of B-GO-*X* MPa and ultrasonicated graphite. (b) EPR spectra of B-GO-*X* MPa and ultrasonicated graphite. (c) B K-edge XANES spectrum of B-GO-16 MPa. (d) IR characterizations of B-GO-*X* MPa and ultrasonicated graphite.

of sp^2 carbon and out-of-plane vibration of sp^3 carbon,[39,40] respectively, the substantial growth of the D band during the SC CO_2/H_3BO_3 treatment indicates conversion of sp^2 hybridized carbon to sp^3, which is consistent with π bond cleavage upon the introduction of the B-hydroxyl group.

Over the π bond cleavage, the potential formation of C-based radical was probed by electron paramagnetic resonance (EPR) spectroscopy. As shown in Fig. 4c, an EPR signal increase at approximately 2.003 was observed as the SC CO_2 pressure increased, which was consistent with the formation of a C-based radical under CO_2/H_3BO_3 treatment. As the presence of unpaired electrons is anticipated when C-based radicals are generated, it can be concluded that when B-hydroxyl is introduced into the graphene motif, π bond cleavage is concomitant with the formation of unpaired electrons. Raman and EPR characterizations show that the introduction of B-hydroxyl leads to π bond cleavage of graphene, which converts sp^2-hybridized C to sp^3. Additionally, unpaired electrons are generated through such a process, as suggested by EPR characterizations.

To further verify the introduction of the B-hydroxyl group into the structure of B-GO-*X* MPa, X-ray absorption near the edge structure spectroscopy (XANES) was performed. According to the B K-edge XANES spectra (Fig. 4d), B 1s → π (194.8 eV) and 1s → σ* (196.4 eV) transitions were observed, and these were proposed to be fingerprint absorptions for B–C and B–OH bonds,[41–43] respectively. The presence of B–OH and B–C bonds was further verified by FT-IR experiments, where absorption bands at 3400, 1100, and 885 cm^{-1} were observed for B-GO-*X* MPa after SC CO_2/H_3BO_3 treatment and were consistent with the stretching frequencies of O–H, B–C, and B–OH bonds, respectively (Fig. 4e).[22,28,44] Thus, the introduction of the –$B(OH)_2$ group into the graphene motif has been proposed.

The magnetic properties of B-GO-*X* MPa were characterized by a superconducting quantum interference device (SQUID) magnetometer. As expected, ultrasonicated pristine graphite in the presence of H_3BO_3 is diamagnetic (Fig. 5a). After SC CO_2 treatment, ferromagnetic hysteresis loops were suggested for B-GO-*X* MPa at 300 K based on the *M*–*H* curves,[5,9,45–48] where the saturation magnetizations (M_s) were characterized to be 0.069, 0.277, and 0.390 emu g^{-1} under treatment with 12, 14, and 16 MPa SC CO_2/H_3BO_3, respectively (Fig. 5a and S5†). Notably, the M_s of B-GO-16 MPa characterized in this work is substantially higher than that of other B-doped graphene in the literature (Table S2†).

Although room-temperature ferromagnetism is suggested by the *M*–*H* curve in Fig. 5a, the coexistence of superparamagnetism and spin-glass cannot be excluded, presumably due to the amorphous nature of the B-GO-*X* MPa system. In addition to M_s, the coercivity (H_c) and residual magnetization (M_r) increases as the SC CO_2 pressure increases and reaches a maximum at 16 MPa (80.03 Oe and 0.018 emu g^{-1}, respectively) (Fig. 5a, inset). The growth of magnetic properties under higher SC CO_2 pressure can be rationalized by the effectiveness of –$B(OH)_2$ introduction. Specifically, because the exfoliation of graphite is expected to be facilitated under elevated SC CO_2 pressure,[25,26] additional C=C bonds are expected to be exposed on the nanosheet surface for alkene addition-derived reaction (Fig. 1b). As a result, introduction of the –$B(OH)_2$ group into the graphene motif will occur with greater efficacy, as evidenced by the XPS and IR results (Fig. 3a and 4d).

With increasing –$B(OH)_2$ concentration, additional unpaired electrons for ferromagnetic coupling are expected to be introduced into the B-GO-*X* MPa system, leading to enhanced magnetism. The room-temperature ferromagnetism of B-GO-16 MPa is characterized by zero-field cooled-field-cooled (ZFC-FC) curves, which merge until the temperature reaches 350 K (Fig. 5b).[49,50] The increase in the ZFC curve from 0 to 100 K suggests the coexistence of the spin-glass state, in addition to the ferromagnetism of B-GO-16 MPa.[51–53]

Density-functional theory (DFT) calculation was used to investigate the origin of the room-temperature ferromagnetism of B-GO-*X* MPa. According to the experimental results, introduction of the –$B(OH)_2$ group and π bond cleavage is expected for B-GO-*X* MPa during the SC CO_2/H_3BO_3 treatment, which is concomitant with the introduction of unpaired electrons. Therefore, a plausible structure of graphene that includes the terminal –$B(OH)_2$ group has been proposed for theoretical magnetic moment investigations.

As shown in Fig. 6a, when terminal –$B(OH)_2$ is introduced into the graphene motif with π bond cleavage, the magnetic moment is characterized to be as high as 0.97 μB, and this is consistent with the significant spin-polarization characterized by spin-resolved total density of states (TDOS) and partial density of states (PDOS) characterizations (Fig. S6†). The TDOS of graphene with terminal –$B(OH)_2$ exhibits a clear asymmetric distribution, due to the inconsistency in the number of spin-up and spin-down electrons.

Interestingly, the net magnetic moment of graphene with terminal –$B(OH)_2$ is significantly higher than those with B substitution alone and B substitution with –OH group introduction, which are relatively well-established structures for B-doped graphene (Fig. 6b–d).[22,54] Therefore, based on experimental and theoretical investigations, the ferromagnetic origin of B-GO-*X* MPa is proposed to be the introduction of –$B(OH)_2$ groups and π bond cleavage during SC CO_2/H_3BO_3 treatment in this work, which effectively removes the p_z orbital of graphene and introduces unpaired spin into the system. Subsequently, the ferromagnetic coupling between these unpaired spins

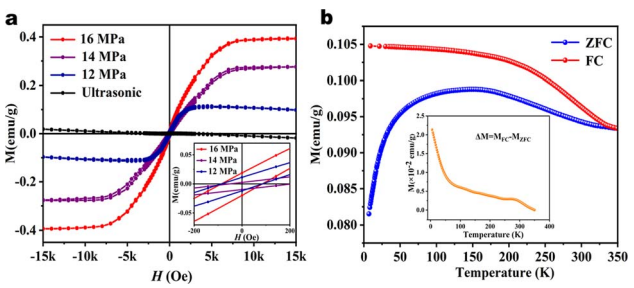

Fig. 5 (a) *M*–*H* curves of B-GO-*X* MPa and ultrasonicated graphite at 300 K. (Inset): *M*–*H* curves near $H = 0$ Oe. (b) FC-ZFC magnetization curves of B-GO-16 MPa at an external magnetic field of 500 Oe. (Inset): $\Delta M = M_{FC} - M_{ZFC}$ curve of B-GO-16 MPa.

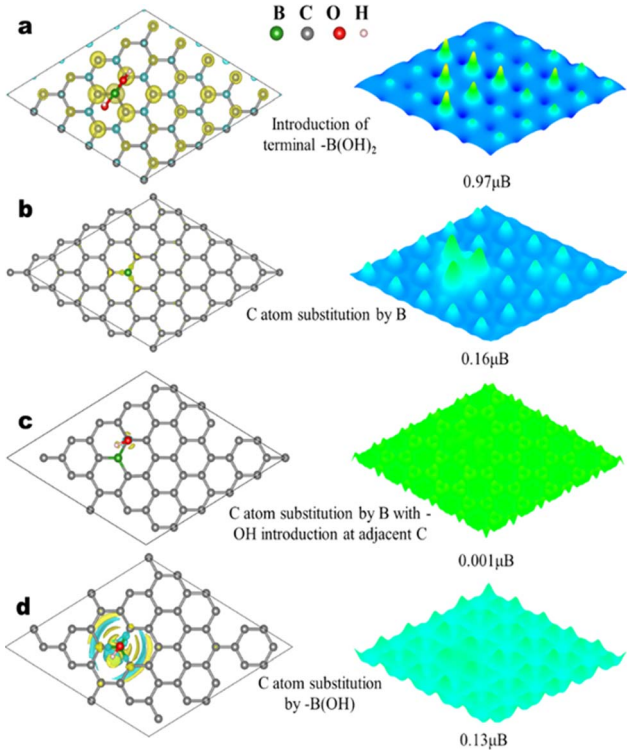

Fig. 6 Spin density distributions and corresponding magnetic moment of (a) graphene with $-B(OH)_2$ introduction and C=C bond cleavage, (b) graphene with B atom substitution, (c) graphene with B atom substitution and –OH group introduction at the C adjacent to B, and (d) graphene with –B(OH) group substitution.

through the conjugated graphene system leads to the as-observed room-temperature ferromagnetism.

Experimental

Materials

Graphite was obtained from Thermo Fisher Scientific Co., Ltd. Hydrogen peroxide (30%) and absolute ethyl alcohol were purchased from Sinopharm Chemical Reagent Co., Ltd (China). Boric acid (H_3BO_3) was purchased from Strem Chemicals (Fluka). Polyvinylpyrrolidone (PVP) was purchased from Strem Chemicals. All other reagents were of analytical grade and were used without further purification. CO_2 with a purity of 99.99% was purchased from Zhengzhou Shuangyang Gas Co. Deionized water was prepared using an ultrapure water apparatus.

Synthesis of B-GO-*X* MPa

The typical experimental steps are as follows. Graphite (200 mg), boric acid (217 mg), and PVP (400 mg) were mixed in anhydrous ethanol (15 mL) and sonicated for 2 h to form a homogeneous dispersion. After the addition of hydrogen peroxide, the mixture was transferred to a supercritical CO_2 apparatus and heated to 80 °C. Subsequently, carbon dioxide was injected into the autoclave under stirring at appropriate pressures (12, 14, and 16 MPa) for the reaction.

After the mixture was reacted for 4 h, the reaction unit was cooled to room temperature and the carbon dioxide was slowly released. The reaction mixture was then sonicated for 30 min, and the products were collected by centrifugation at 5000 rpm for 15 min at room temperature to remove aggregates. The precipitate was collected in a tube and centrifuged at 10 000 rpm for 20 min to remove the PVP and H_2O_2. After centrifugation at 10 000 rpm, the precipitates were combined and washed four times with ethanol before being dried in a vacuum oven at 60 °C overnight.

Characterization

The morphology and structure of the samples were characterized by field emission SEM (JEORJSM-6700F), AFM (Nanoscope IIIA), TEM (JEOL JEM 2100), and HRTEM. X-ray diffraction (XRD) patterns were collected using a Bruker D8 Focus diffractometer (Bruker AXS, Germany) with Cu K-radiation. Raman spectra were recorded on a Renishaw microscope system RM2000 with a laser wavelength of 532 nm. X-ray absorption near edge structure (XANES) measurements were conducted at the insertion-device beamline of the Materials Research Collaborative Access Team (MRCAT) at the Advanced Photon Source located within the National Synchrotron Radiation Laboratory. The energy resolution for the absorption spectra is approximately 40 and 80 meV for the boron edges, respectively.

Computational methods

All the calculations were based on density functional theory (DFT) as implemented in the Vienna *Ab initio* Simulation Package (VASP) code utilizing the projector augmented wave (PAW) method. The exchange–correlation energy of generalized gradient approximation proposed by Perdew, Burke, and Ernzerhof (GGA-PBE) was adopted. A vacuum of 20 Å perpendicular to the sheets was applied to avoid interaction between the layers. A kinetic energy cut-off of 450 eV was used for the plane-wave basis set. The sampling in the Brillouin zone was set at $5 \times 5 \times 1$ by the Monkhorst–Pack method. The convergence criteria employed for the electronic self-consistent relaxation and ionic relaxation were set at 10^{-4} and 0.02 eV $Å^{-1}$ for energy and force, respectively.

Conclusions

Terminal $-B(OH)_2$ introduction and π bond cleavage were simultaneously achieved for a 2D graphene system *via* a facile SC CO_2/H_3BO_3 treatment, which effectively converted the sp^2 and p_z orbitals of graphene to sp^3. As a result, unpaired electrons were introduced into the graphene motif, which led to room-temperature ferromagnetism with saturation magnetization up to 0.390 emu g^{-1} as well as coercivity (H_c) and residual magnetization (M_r) estimated to be 80.03 Oe and 0.018 emu g^{-1}, respectively. Theoretical investigations suggest that the introduction of the $-B(OH)_2$ group and cleaving of the π bond of graphene can induce a magnetic moment more effectively compared to conventional B substitution and –OH introduction. In addition to providing a novel approach to modulate the

magnetic properties of a graphene motif, we anticipate that this work will provide a thorough understanding of the magnetic origin of 2D-conjugated materials.

Data availability

The data supporting this article have been included as part of the ESI.†

Author contributions

D. Zhang conducted the major experiments and collected data. B. Gao conducted computational investigations. Y. Ouyang conducted part of the experiments and revised the manuscript. S. Xu interpreted the data and revised the manuscript. Q. Tian and W. Wu revised the manuscript. Q. Xu designed the project and experiments.

Conflicts of interest

The authors declare no competing interests.

Acknowledgements

We are grateful to the National Natural Science Foundation of China (No. 51173170, 21703207, 21773216), the joint project from the Henan-Provincial and the China-National Natural Science Foundation (Project No. U2004208), the Central Plains Science and Technology Innovation Leading Talent Project (Project No. 234200510008) and Natural Science Foundation of Henan Province of China (Project No. 242300421600).

Notes and references

1 I. Žutić, J. Fabian and S. Das Sarma, *Rev. Mod. Phys.*, 2004, **76**, 323.
2 A. Soumyanarayanan, N. Reyren, A. Fert and C. Panagopoulos, *Nature*, 2016, **539**, 509.
3 Y. Wan, X. Cheng, Y. Li, Y. Wang, Y. Du, Y. Zhao, B. Peng, L. Dai and E. Kan, *RSC Adv.*, 2021, **11**, 4035.
4 B. Wu, S. Gao, W. Xue, S. Li and D. Duan, *Ceram. Interfaces*, 2021, **47**, 5019.
5 N. Wang, H. Tang, M. Shi, H. Zhang, W. Zhuo, D. Liu, F. Meng, L. Ma, J. Ying, L. Zou, Z. Sun and X. Chen, *J. Am. Chem. Soc.*, 2019, **141**, 17166.
6 M. V. Koudriachova, S. W. de Leeuw and N. M. Harrison, *Phys. Rev. B: Condens. Matter Mater. Phys.*, 2004, **69**, 054106.
7 I. V. Solovyev, *Phys. Rev. B: Condens. Matter Mater. Phys.*, 2006, **74**, 054412.
8 C. N. R. Rao, H. S. S. R. Matte, K. S. Subrahmanyam and U. Maitra, *Chem. Sci.*, 2012, **3**, 45.
9 Y. Li, X. Cheng, Y. Zhao, M. Liu, F. Li, C. Huang, L. Dai, Y. Wan and E. Kan, *J. Phys. Chem. C*, 2023, **127**, 12648.
10 J. J. Palacios, J. Fernández-Rossier and L. Brey, *Phys. Rev. B: Condens. Matter Mater. Phys.*, 2008, **77**, 195428.
11 J. Tuček, K. Holá, A. B. Bourlinos, P. Błoński, A. Bakandritsos, J. Ugolotti, M. Dubecký, F. Karlický, V. Ranc, K. Čépe, M. Otyepka and R. Zbořil, *Nat. Commun.*, 2017, **8**, 8.
12 L. Ma, H. Hu, L. Zhu and J. Wang, *J. Phys. Chem. C*, 2011, **115**, 6195.
13 P. Błoński, J. Tuček, Z. Sofer, V. Mazánek, M. Petr, M. Pumera, M. Otyepka and R. Zbořil, *J. Am. Chem. Soc.*, 2017, **139**, 3171.
14 S. S. Kim, H. S. Kim, H. S. Kim and Y.-H. Kim, *Carbon*, 2015, **81**, 339.
15 H. González-Herrero, J. M. Gómez-Rodríguez, P. Mallet, M. Moaied, J. J. Palacios, C. Salgado, M. M. Ugeda, J.-Y. Veuillen, F. Yndurain and I. Brihuega, *Science*, 2016, **352**, 437.
16 J. Ge, T. Luo, Z. Lin, J. Shi, Y. Liu, P. Wang, Y. Zhang, W. Duan and J. Wang, *Adv. Mater.*, 2020, **33**, 2005465.
17 P. Wahl, P. Simon, L. Diekhöner, V. S. Stepanyuk, P. Bruno, M. A. Schneider and K. Kern, *Phys. Rev. Lett.*, 2007, **98**, 056601.
18 J. Zhao, H. Zeng and J. W. Wei, *Phys. Rev. B: Condens. Matter Mater. Phys.*, 2012, **407**, 204.
19 H. Tachikawa and H. Kawabata, *J. Phys. Chem. C*, 2009, **113**, 7603.
20 E. H. Lieb, *Phys. Rev. Lett.*, 1989, **62**, 1201.
21 H. C. Brown and C. F. Lane, *J. Am. Chem. Soc.*, 1970, **92**, 6660.
22 L. Du, B. Gao, S. Xu and Q. Xu, *Nat. Commun.*, 2023, **14**, 2278.
23 C. Gómez-Navarro, J. C. Meyer, R. S. Sundaram, A. Chuvilin, S. Kurasch, M. Burghard, K. Kern and U. Kaiser, *Nano Lett.*, 2010, **10**, 1144.
24 S. H. Dave, C. Gong, A. W. Robertson, J. H. Warner and J. C. Grossman, *ACS Nano*, 2016, **10**, 7515.
25 Y. Li, L. Zhang, Q. Tian and Q. Xu, *Curr. Opin. Green Sustainable Chem.*, 2021, **28**, 100424.
26 Y. Qi, Q. Xu, Y. Wang, B. Yan, Y. Ren and Z. Chen, *ACS Nano*, 2016, **10**, 2903.
27 M. A. Vieira, G. R. Gonçalves, D. F. Cipriano, M. A. Schettino, E. A. Silva Filho, A. G. Cunha, F. G. Emmerich and J. C. C. Freitas, *Carbon*, 2016, **98**, 496.
28 S. K. Sarkar, K. K. Raul, S. S. Pradhan, S. Basu and A. Nayak, *Phys. E*, 2014, **64**, 78.
29 K. Krishnamoorthy, M. Veerapandian, K. Yun and S. J. Kim, *Carbon*, 2013, **53**, 38.
30 L. Du, S. Cao, X. Zheng, L. Jiang, Z. Ren, J. Chen and Q. Xu, *Macromol. Mater. Eng.*, 2020, **305**, 2000172.
31 T. V. Khai, H. G. Na, D. S. Kwak, Y. J. Kwon, H. Ham, K. B. Shim and H. W. Kim, *Chem. Eng. J.*, 2012, **211–212**, 369.
32 D.-Y. Yeom, W. Jeon, N. D. K. Tu, S. Y. Yeo, S.-S. Lee, B. J. Sung, H. Chang, J. A. Lim and H. Kim, *Sci. Rep.*, 2015, **5**, 9817.
33 A. Pakdel, Y. Bando and D. Golberg, *ACS Nano*, 2014, **8**, 10631.
34 J. Zhu, T. Diao, W. Wang, X. Xu, X. Sun, S. A. C. Carabineiro and Z. Zhao, *Appl. Catal., B*, 2017, **219**, 92.
35 N. Meng, J. Ren, Y. Liu, Y. Huang, T. Petit and B. Zhang, *Energy Environ. Sci.*, 2018, **11**, 566.
36 S. Sarkar, R. Roy, B. K. Das and K. K. Chattopadhyay, *Carbon*, 2021, **184**, 253.

37 M. Z. Iqbal, G. Hussain, S. Siddique, M. W. Iqbal, G. Murtaza and S. M. Ramay, *J. Magn. Magn. Mater.*, 2017, **422**, 322.
38 S. Sarma, S. C. Ray and A. M. Strydom, *Diamond Relat. Mater.*, 2017, **79**, 1.
39 K. N. Kudin, B. Ozbas, H. C. Schniepp, R. K. Prud'homme, I. A. Aksay and R. Car, *Nano Lett.*, 2008, **8**, 36.
40 D. B. Schüpfer, F. Badaczewski, J. Peilstöcker, J. M. Guerra-Castro, H. Shim, S. Firoozabadi, A. Beyer, K. Volz, V. Presser, C. Heiliger, B. Smarsly and P. J. Klar, *Carbon*, 2021, **172**, 214.
41 C. Tang, L. Zhang, S. Sanvito and A. Du, *J. Mater. Chem. C*, 2020, **8**, 7034.
42 R. Gago, I. Jiménez, x. I. a. Garcı and J. M. Albella, *Vacuum*, 2002, **64**, 199.
43 Y. Tison, J. Lagoute, V. Repain, C. Chacon, Y. Girard, S. Rousset, F. Joucken, D. Sharma, L. Henrard, H. Amara, A. Ghedjatti and F. Ducastelle, *ACS Nano*, 2015, **9**, 670.
44 J. Yang, B. Gao, W. Liu, J. Du and Q. Xu, *ChemPhysChem*, 2023, **24**, e202200793.
45 R. Chen, F. Luo, Y. Liu, Y. Song, Y. Dong, S. Wu, J. Cao, F. Yang, A. N'Diaye, P. Shafer, Y. Liu, S. Lou, J. Huang, X. Chen, Z. Fang, Q. Wang, D. Jin, R. Cheng, H. Yuan, R. J. Birgeneau and J. Yao, *Nat. Commun.*, 2021, **12**, 3952.
46 Z. Guguchia, A. Kerelsky, D. Edelberg, S. Banerjee, F. von Rohr, D. Scullion, M. Augustin, M. Scully, D. A. Rhodes, Z. Shermadini, H. Luetkens, A. Shengelaya, C. Baines, E. Morenzoni, A. Amato, J. C. Hone, R. Khasanov, S. J. L. Billinge, E. Santos, A. N. Pasupathy and Y. J. Uemura, *Sci. Adv.*, 2018, **4**, eaat3672.
47 P. Sun, K. Wang, J. Wei, M. Zhong, D. Wu and H. Zhu, *Nano Res.*, 2014, **7**, 1507.
48 C. Liu, Y. Yang, Z. Ma, C. Zhou, D. Liu, X. Luo, X. Zhu, Y. Sun and Z. Sheng, *J. Phys. Chem. C*, 2020, **124**, 7396.
49 S. Lu, L. Sui, M. Wu, S. Zhu, X. Yong and B. Yang, *Adv. Sci.*, 2019, **6**, 1801192.
50 Q. Lu, Q. Zhao, T. Yang, C. Zhai, D. Wang and M. Zhang, *ACS Appl. Mater.*, 2018, **10**, 12947.
51 M. J. Benitez, O. Petracic, E. L. Salabas, F. Radu, H. Tüysüz, F. Schüth and H. Zabel, *Phys. Rev. Lett.*, 2008, **101**, 097206.
52 H. Khurshid, P. Lampen-Kelley, Ò. Iglesias, J. Alonso, M.-H. Phan, C.-J. Sun, M.-L. Saboungi and H. Srikanth, *Sci. Rep.*, 2015, **5**, 15054.
53 D. Peddis, K. N. Trohidou, M. Vasilakaki, G. Margaris, M. Bellusci, F. Varsano, M. Hudl, N. Yaacoub, D. Fiorani, P. Nordblad and R. Mathieu, *Sci. Rep.*, 2021, **11**, 7743.
54 Y. A. Kim, K. Fujisawa, H. Muramatsu, T. Hayashi, M. Endo, T. Fujimori, K. Kaneko, M. Terrones, J. Behrends, A. Eckmann, C. Casiraghi, K. S. Novoselov, R. Saito and M. S. Dresselhaus, *ACS Nano*, 2012, **6**, 6293.